Arch. Metall. Mater. **66** (2021), 4, 1141-1148

DOI: 10.24425/amm.2021.136434

S. ARUL[1*], T. SENTHILNATHAN[2], V. JEEVANANTHAM[3], K.V. SATHEESH KUMAR[4]

PSEUDOCAPACITIVE CHARACTERISTICS OF Mg DOPED ZnO NANOSPHERES PREPARED BY COPRECIPITATION

A n-type semiconductor ZnO has high transmittance features, excellent chemical stability and electrical properties. It is also commonly used in a range of fields, such as gas sensors, photocatalysts, optoelectronics, and solar photocell. Magnesium-doped zinc oxide (Mg-ZnO) nano powders were effectively produced using a basic chemical precipitation process at 45°C. Calcined Mg-ZnO nano powders have been characterized by FTIR, XRD, SEM-EDX and PL studies. XRD measurements from Mg-ZnO revealed development of a crystalline structure with an average particle size of 85 nm and SEM analysis confirmed the spherical morphology. Electrochemical property of produced Mg-ZnO nanoparticles was analyzed and the specific capacitance value of 729 F g^{-1} at 0.5 A g^{-1} current density was recorded and retained a specific capacitance ~100 percent at 2 A g^{-1} current density.

Keywords: Zinc Oxide, Mg-doped ZnO, Coprecipitation, Cyclic Voltammetry, EIS

1. Introduction

Semiconductor nanoparticles show a significant role in advanced research into the handling and distribution of simple resources for energy storage systems, magnetic systems, photocatalytic and biocompatible applications [1-4]. Although there are several reports available for the creation of metal oxide nanoparticles (ZnO, NiO, Al_2O_3, TiO_2, SnO_2, etc) and their photocatalytic and electrochemical properties, the additional studies will enhance the making of metal oxide-based nanoparticles [5-9]. Ultracapacitor's capacity to deliver high-power bursts over a shorter period of time relative to other storage devices was confirmed through applications in power systems, cars, solar cells, etc [10-13]. Carbon materials are the most commonly used conductor material due to its high specific area and low internal resistance and, similarly, metal oxides (ZnO, SnO_2 and TiO_2) which also have theoretical specific ability that can be used as a substitute [14-16]. ZnO is an n-type semiconductor with exceptional characteristics in the applications of electronics, chemicals and optometry due to its significant properties such as wide band gap of 3.3 eV at room temperature (RT) and high exciton binding energy (60 meV). Moreover, zinc oxide with high thermal and chemical stability, low expense, non-toxic, clear doping, paid considerable interest in building supercapacitors [17]. Ezhil Arasi and his team successfully synthesized nanostructured zinc vanadate, $Zn_3(VO_4)_2$, using a simple co-precipitation process and recorded an exclusive capacity of 312 F / g with high retention rate of approximately 90.7 percent after the 5000th cycle [18]. Hybrid MnO-coated ZnO nanorods arrays successfully synthesised by chemical bath deposition and examined surface morphology and precise capacitance [19]. Zincite/ carbon nanocomposite formed by the addition of sugar solution to dicarbomethoxyzinc and its magnetic, electrochemical properties have been evaluated [20]. A green method reported by taking ZnO and TiO_2 from Kaffir Lime and Ilmenite Mineral, respectively, and their composite is prepared in the existence of SWNT's (single walled nanotube's) for the full use of electrochemically active nanomaterial for energy storage [21].

Guoyanwu and his colleagues reported the preparation of ZnO/N-OHPC and its application as a supercapacitor anode [22]. This is an example of a hybrid energy storage device that incorporates open-cell foam of graphene and ZnO electrodes to provide high energy capacity while simultaneously showing both high power density and high capacitance [23]. ZnO 's realistic usage as an electrode material is limited due to poor conductivity and a broad volume impact in the charging and discharge

[1] JAI SHRIRAM ENGINEERING COLLEGE, DEPARTMENT OF PHYSICS, TIRUPUR-638660, TAMILNADU, INDIA
[2] SRI VENKATESHWARA COLLEGE OF ENGINEERING, DEPARTMENT OF APPLIED PHYSICS, SRIPERUMBUDUR-602117, TAMILNADU, INDIA
[3] VIVEKANANDHA COLLEGE OF ARTS & SCIENCES FOR WOMEN, DEPARTMENT OF CHEMISTRY, TIRUCHENGODE 637205, TAMILNADU, INDIA
[4] KONGU ENGINEERING COLLEGE, DEPARTMENT OF MECHANICAL ENGINEERING, ERODE-638060, TAMILNADU, INDIA

* Corresponding author: kirthickarul@gmail.com

phase [24]. In comparison, MgO has strong electrical stability, load storage strength, porosity and provides a way to intercalate electrolytic ions into working materials. There are not lot of magnesium-doped ZnO nanomaterials synthesis studies and their supercapacitor implementations. This research describes the preparation including electrochemical properties of magnesium doped ZnO nanopowders through chemical precipitation. The substitution of magnesium in zinc oxide reduces the nanosize, which may improve significant performance of electrode conductivity of ZnO and influences in the charging and discharge phase.

2. Experimental

Critical chemicals for the synthesis of ZnO nanopowders by soft chemical process have been obtained from Merck used without purification and deionized water used as solvent for solution. (1 M) Zn $(NO)_3$ and magnesium nitrate hexahydrate (0.05 M) have been utilized as precursors for the synthesis. The salts were solubilized in 100 ml of deionized water in a magnetic stirrer for half an hour. NaOH solution (2 M) was diluted with the starting solution to obtain a large volume of white precipitate under continuous 45°C stirring. Using purified water, the precipitates were filtered and washed for 4 hours in a hot air oven at 120°C and powdered in agar mortar. The final powder was calcined for 3 hours at 450°C and permitted to cool in the oven (Fig. 1).

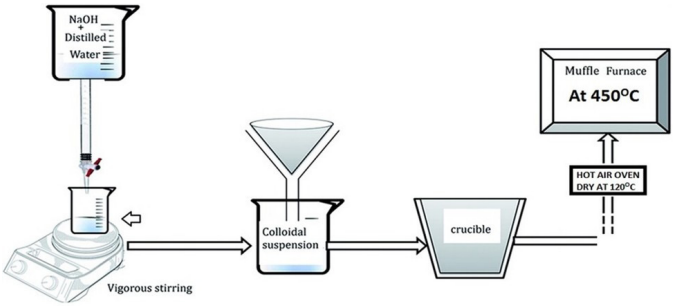

Fig. 1. Schematic diagram of preparation of nanoshpere calcinated at 450°C

Further characterization studies have been performed on the collected nanopowders. The FT-IR spectra were reported between the wavenumbers of 4000-400 cm^{-1} using the SHIMADZU FTIR 8400S spectrometer by mixing the samples evenly with KBr. XRD patterns attained in the 2theta range from 10-80° using BRUKER, Germany, Model-D8-Advance diffractometer operating with Cu-Kш radiation ($\lambda = 0.154060$ nm). The particle size averages determined by the formula of Debye Scherrer Eq. (1)

$$D = \frac{0.9\lambda}{\beta \cos\theta} \tag{1}$$

Here,

D – particles size average,

λ – wavelength of the X-ray source,

β – full-width at half-maximum (FWHM) and

θ – diffraction angle of Bragg.

Lattice parameters a and c of Mg-doped Zinc oxide samples were determined from (100) and (002) centered X-ray diffraction peaks using the equation Eq. (2) and Eq. (3)

$$a = \frac{\lambda}{\sqrt{3}\sin\theta} \tag{2}$$

$$c = \frac{\lambda}{\sin\theta} \tag{3}$$

The assessment of basic electrochemical ability can be carried out by implementing the given term Eq. (4)

$$\Delta C_s = \frac{I}{m}\frac{\Delta t}{\Delta V} \tag{4}$$

Here, I cathode current applied, when t – discharge time, m – active material mass, and V – applied potential window. The surface structures of the samples were attained from the JEOL JSM 6390LV high-performance, low-cost electron microscope with a high resolution of 3.0 nm. Using an ultra-sonication powder samples dispersed in deionized water, PL spectra were collected using a Perkin-Elmer PL spectrometer with an excitation wavelength of 260 nm. The following technique was applied to prepare Zn-MgO as a working electrode, where open cell foam of nickel was cleaned in 3 M aqueous HCl solution for half an hour under ultrasound. The open cell foam of nickel was then additionally washed with distilled H_2O followed by C_2H_5OH and dried at 80°C for 12 h in hot air oven. A 4 mg concentration of the active compound was coated on nickel foam and used to create a semi-liquid combination of the active compound. AC (Activated carbon) and polyvinylidene fluoride (PVDF) at 8:1:1 ratio with N-methyl-2-pyrrolidone (NMP) was utilized as a solvent. The semi-liquid mixture was coated to unit (1 cm × 1 cm) through a drop casting process and dried at 80°C in hot air for half a day. Here, Ni-foam mounted on active material behaves as a working electrode; platinum wire as counter electrode and Ag/AgCl electrode as reference electrodes with 2M Potassium Hydroxide solution as electrolytes respectively.

3. Result and discussion

Fig. 2 shows the infrared spectra of prepared undoped ZnO and Mg-doped Zinc oxide nano- sized particles and the bands viewed at 543.09 cm^{-1} and 547.65 cm^{-1}, of undoped ZnO and Mg-doped ZnO nanoparticles proves metal oxides. Peaks at 1384.26 cm^{-1} and 1580 cm^{-1} appeared for undoped ZnO and Mg-doped ZnO nanoparticles were due to bent oxygen stretching frequency mode. The existence of peak about 3445.12 cm^{-1} for undoped ZnO, in addition the band at 3445.19 cm^{-1} of Mg doped ZnO were due to O-H stretching vibrations. From the above inference, variations in the peak shifts affirms the occurrence of Mg doped ZnO lattice [25].

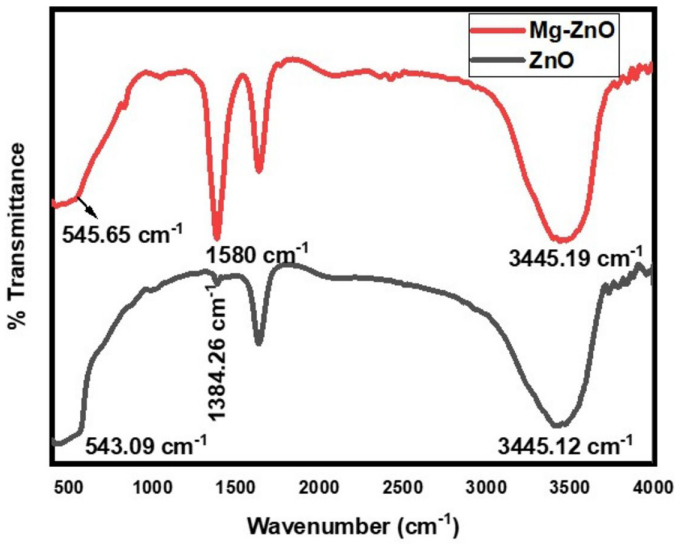

Fig. 2. FTIR spectra of ZnO and Mg-ZnO calcinated at 450°C

Fig. 3 presents the XRD pattern of Mg-ZnO nanoparticles synthesized by soft chemical process and calcined at 450°C. Both diffraction peaks corresponded to the hexagonal wurtzite structure of zinc oxide (JCPDS No. 36-1451). Diffraction shows that dopant addition does not lead to secondary phases and the x-ray diffraction pattern of Mg-doped NPs remains unchanged, manganese ions are doped into the ZnO, and hence, a tiny amount of strain is influenced. The peaks 2θ = 31.44°, 34.37°, 35.92°, 47.22°, 56.41°, 63.08°, 66.30°, 67.71° and 68.89° corresponding to (100), (002), (101), (102), (110), (103), (200), (112), and (201) planes of Mg-ZnO are of high intensity and the diffraction intensity increases because of the incorporation of magnesium. Most of the Mg^{2+} ions substitution in the lattice to fill in the voids. Therefore, the original wurtzite structure of Zn nanoparticles is not altered even when Mg-ZnO Nanosized particles are formed [26]. The average particle size of Mg-ZnO nanoparticles measured as 85 nm [27]. The lattice parameters of the Mg doped ZnO specify the existence of doping MgO with values a = 3.25Å, c = 5.213 Å and c/a = 1.602 Å, as the difference is due to the lower ion radius of Mg than Zn.

The images of Mg-doped ZnO nanoparticles (Fig. 4a) displays that the prepared nanoparticles were non-uniform in size and almost sphere-shaped in morphology. The image shows the agglomeration was taken place and the nanoparticle size of Mg-ZnO was measured to be around 85 nm, which was agree well with XRD [28].

Fig. 4b indicates the EDX spectra of Mg-doped ZnO nanoparticles and specifies the presence of zinc and oxygen elements, further, Mg in the host lattice and also indicates the nonappearance of impurities connected with the XRD analysis. The higher peak in the spectrum indicates high concentration of the ingredient in doped nanomaterials. Fig. 4b indicates higher peaks Zn element than the associated elements of Mg and O [29,30].

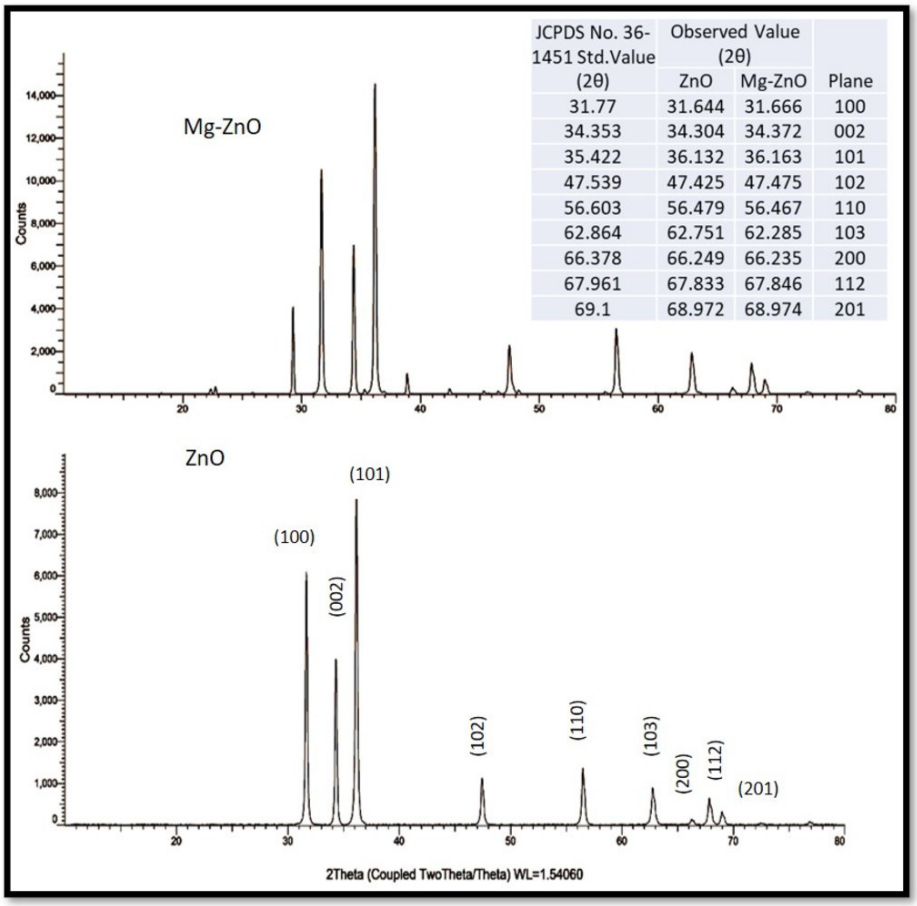

Fig. 3. X-ray diffractions of undoped ZnO and Mg-ZnO calcinated at 450°C

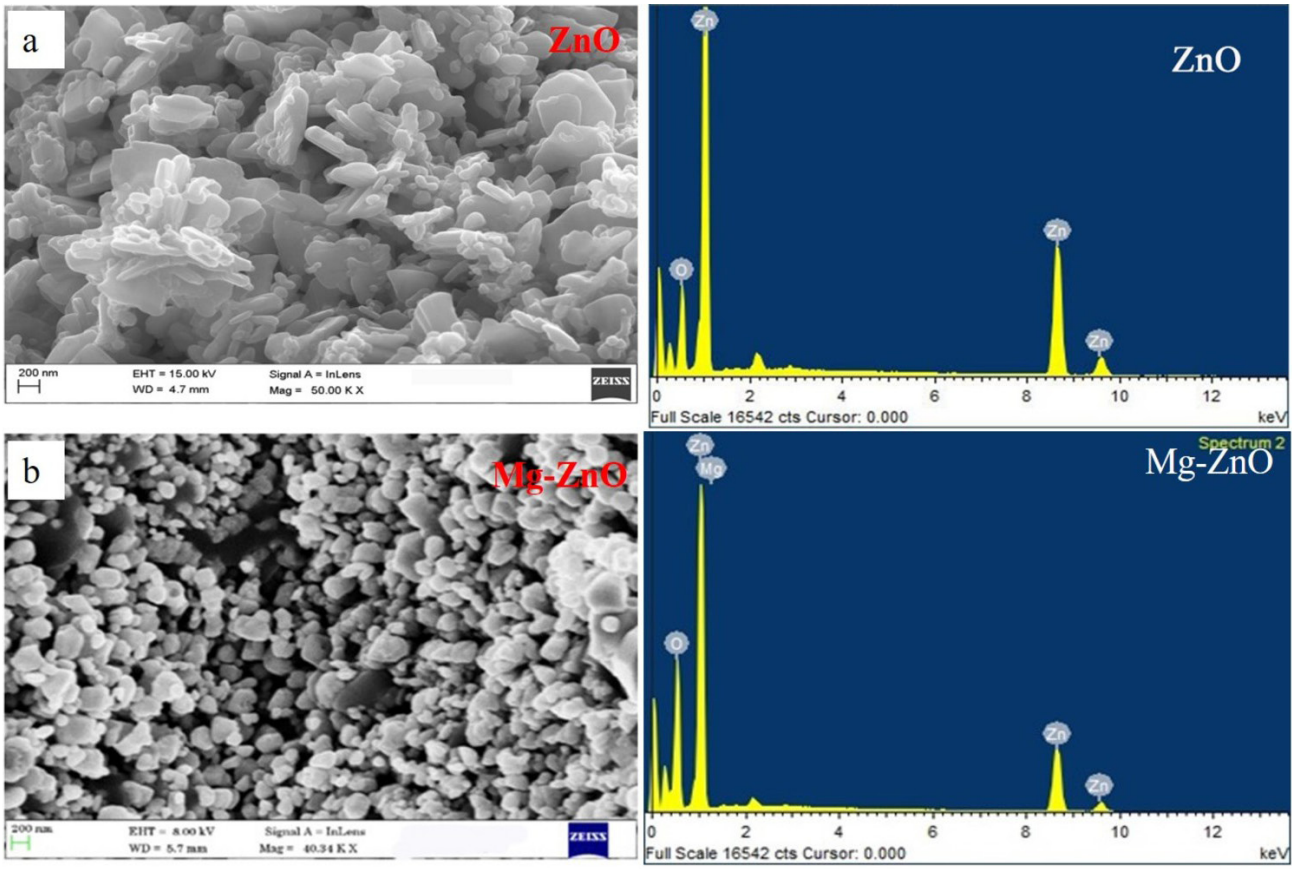

Fig. 4. (a) SEM and (b) EDX images of ZnO and Mg-ZnO calcinated at 450°C

Fig. 5a shows the UV-Vis spectra of pure zinc oxide and Mg-ZnO nano samples. The λ (wavelength) for prepared nano-sized samples was 326 nm for undoped ZnO and 328 nm, Mg-doped ZnO nanoparticles respectively. The characteristic peaks assigned to intrinsic bandgap absorption of pure zinc oxide and Mg-ZnO nano samples. This could be because of surface-bound electrons tunnelling into holes that are already there. The strength of emission bands decreases as the Mg content of the sample is raised, which blocks the recombination of photo-generated electrons and holes. Moreover, Mg ions serve as additional active defect sites within the ZnO lattice, producing additional visible light adsorption as a result. Fig. 5b depicts the optical characters of the synthesized undoped ZnO and Mg-ZnO tested using a photo-luminescent spectrum that is excited at a wavelength of 270 nm. The straight recombination of the exciton-exciton collision process for Mg-doped ZnO samples occurred at 465 nm and was attributable to a high near-band edge emission peak [31]. The absorption peak rises with the quantity of Mg that is added. It is likely that different causes, such as particle size, lack of oxygen, and grain structure defects,

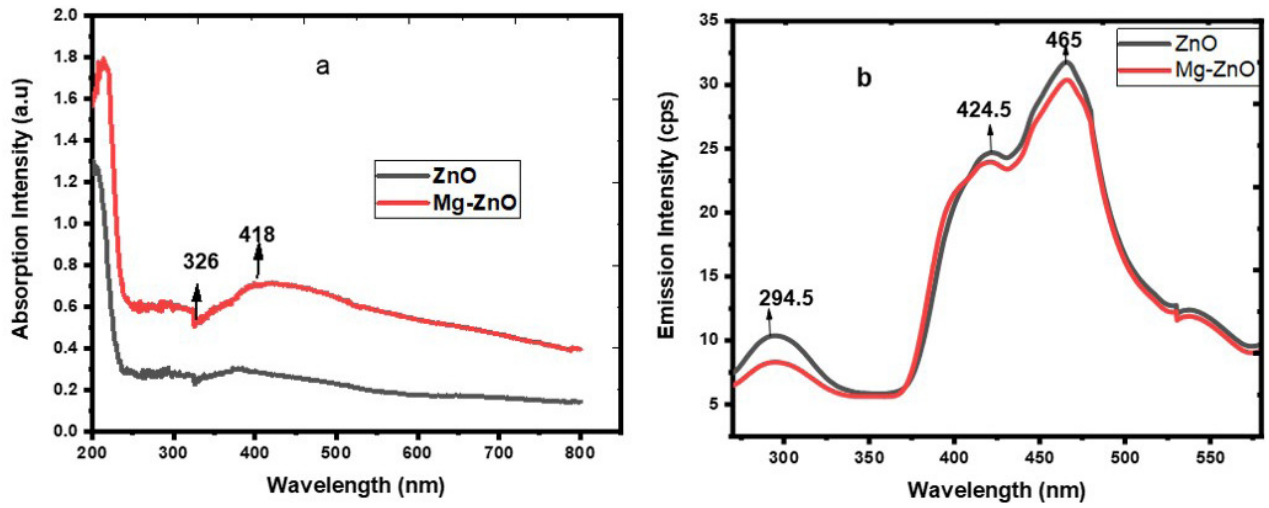

Fig. 5. (a) UV-Vis absorbance and (b) PL spectra of ZnO along with Mg-ZnO calcinated at 450°C

may lead to the rise in absorbance. When it comes to Mg-doped ZnO nanoparticles, a large degree of absorption is observed in between 380 nanometers and 600 nanometers, although very little absorption is seen in the visible zone, as shown in the image (Fig. 5b). The molecules in the lower energy state are excited to the higher energy states, allowing greater absorption of photon energy. Therefore, it is clear from the aforementioned results that the coprecipitation formed nanostructured Mg-doped ZnO with superior textural properties.

The electrochemical behaviors of undoped ZnO and Mg-doped zinc oxide and the following approaches, such as cyclic voltammetry, electroimpedence (EIS) and galvanostatic charging and discharging (GCD), were used to discuss the electrochemical properties of Mg-doped ZnO.

Fig. 6a shows the undoped ZnO and Mg-ZnO CV curves, once the scan rate varies from 10-100 mV/s under 0-0.6 V potential window in (1 M) KOH electrolyte solution. CV of bare nickel foam was previously tested for active sample and the tests were related to the active sample, which was appeared to be poor for bare nickel. As the rate of scanning increased from 10-100 mV/ s, the redox peak change was observed and cyclic-voltametric curves show the oxidation peak of Zn^{2+} and Zn^{3+} in the anodized and reduction peaks of – 0-0.6 V cathodic region. Further, the linear increase in redox current peaks with a rising scan rate suggests the process in transfer of charges at the interface due to redox effects and a quick increase in the rate of mobility in electrons and ions [32-34]. The pseudo-capacitive aspect of the zinc oxide and Mg-ZnO are clearly evident from the above findings and was as a result of the faradic effectiveness between the particles in the electrolytic solution and the electrical loads on the surface of the working materials. The pseudo-capacitive activity of undoped ZnO and Mg-doped ZnO shows a higher capacitive existence, which may be attributed to the creation of standardized and complete nanosphere structure discovered from SEM images, and it improves the intercalation between the charge carriers in the electrolyte to the working electrode. It is therefore important to remember that these pseudo-capacity behaviors for undoped ZnO and Mg-ZnO could be attributed to nano-sized spheres exposure. Fig. 6b includes EIS synthesized ZnO and Mg-doped ZnO nanosphere Nyquist plots. Electrochemical interface resistance, consisting of internal active material sensitivity, electrolyte ion sensitivity and boundary interaction resistance between electrode and electrolyte, resulted from EIS juncture curves. Furthermore, the parallel curve with the same slope in the low frequency spectrum shows similar ion diffusion properties.

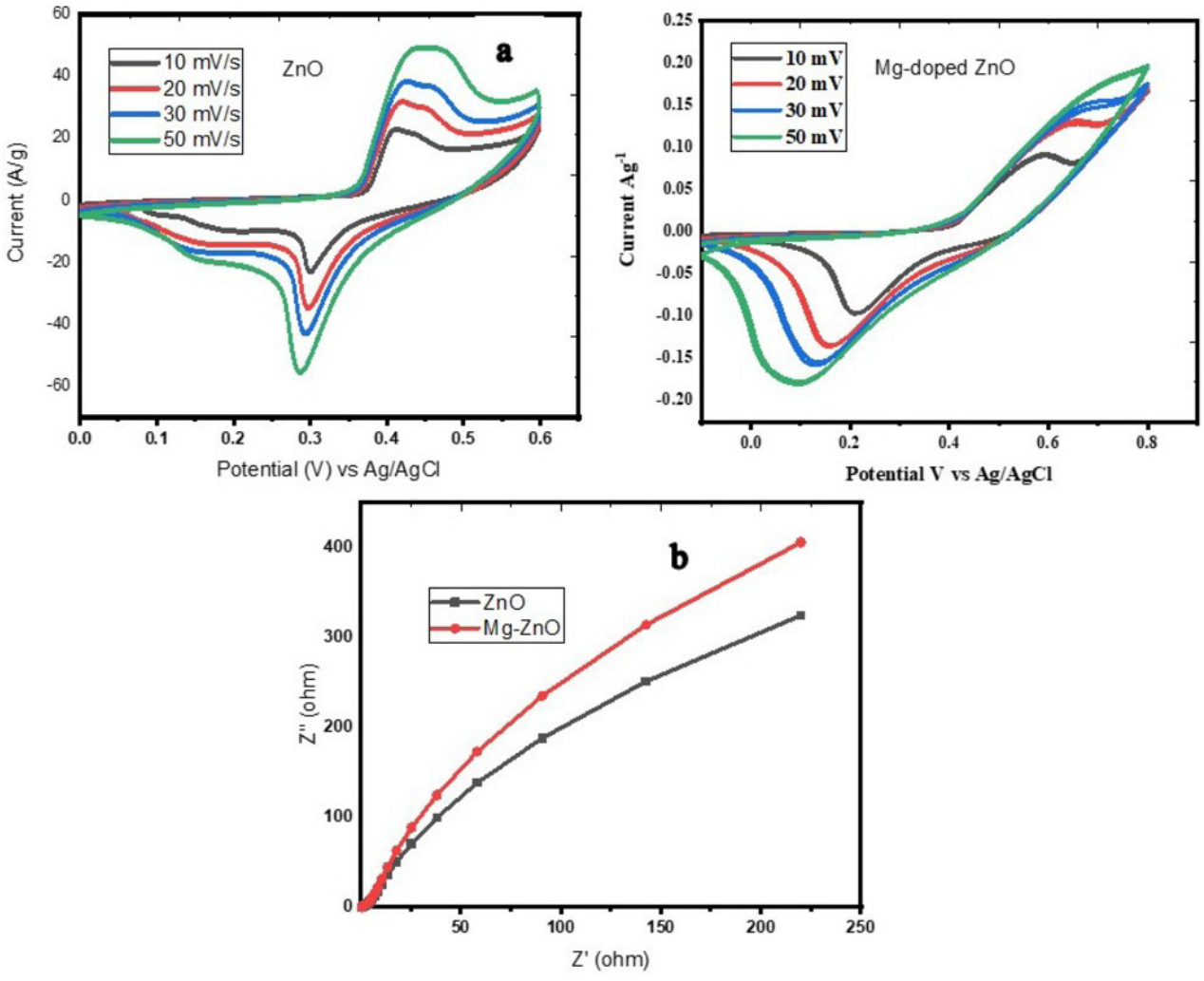

Fig. 6. (a) CV curves and (b) EIS spectra of Mg-ZnO calcined at 450°C

With the aim of exploring the capacitive behavior of the undoped Zinc oxide and Mg-ZnO galvanostatic charging and discharging tests, at current densities of 0.5-3 and 5 A g^{-1} were completed with the –1-0.5 V potential window (Fig. 7a). That shows asymmetric pattern of charging and unloading curves. Faradic electron transfer and IR (internal drop resistance) of the active material was responsible for nonlinearity and the existence of the high-level region occurred at the start of the discharge cycle [35].

The determined specific capacitance of the samples obtained at varying current densities is shown in Table 1. The incomplete formation of spheres was a characteristic feature of Mg-doped ZnO, which allows the transporter to enter the active sites and was well assisted by its unique capability. The observed superior capacitance of Mg-doped ZnO might be due to nanoscale spheres, which increase the contact between the active site and the charge carrier in the electrolyte. The constant existence of the specific capacitance of Mg-doped ZnO at current densities 1-2 A g^{-1} is clearly shown.

It's clear from the Fig. 7b. that the Mg-doped ZnO has an equal discharge form and a specific capacitance 0.5-5 A g^{-1}. The calculated specific capacitance of ZnO and Mg-doped ZnO

TABLE 1

Measured specific capacitance of Mg-doped ZnO at varying current density

Potential window (V)	Current density (Ag^{-1})	Specific capacitance (Fg^{-1})	
		ZnO	Mg-ZnO
0.5	0.5	213.6	729
0.5	1	220	662
0.5	2	200	618.4
0.5	3	240	481.8
0.5	5	100	338

are 213.6 F g^{-1} and 729 F g^{-1} at 0.5 A g^{-1} current density and retained their specific capacitance (200 F g^{-1} and 618.4 F g^{-1}) of 100 percent at current density 2 A g^{-1}. It is clearly evident that addition of magnesium to ZnO increases the specific capacitance.

The stability measurement was considered as a significant study to be performed to inspect the stability of materials. The compatible chronopotentiometry technique Mg-doped ZnO cyclic test for 500 cycles was tested in a 3-electrode device shown in Fig. 8. That elucidates the galvanostatic charge/discharge curves for the initial and final few cycles of the 500 galvanostatic

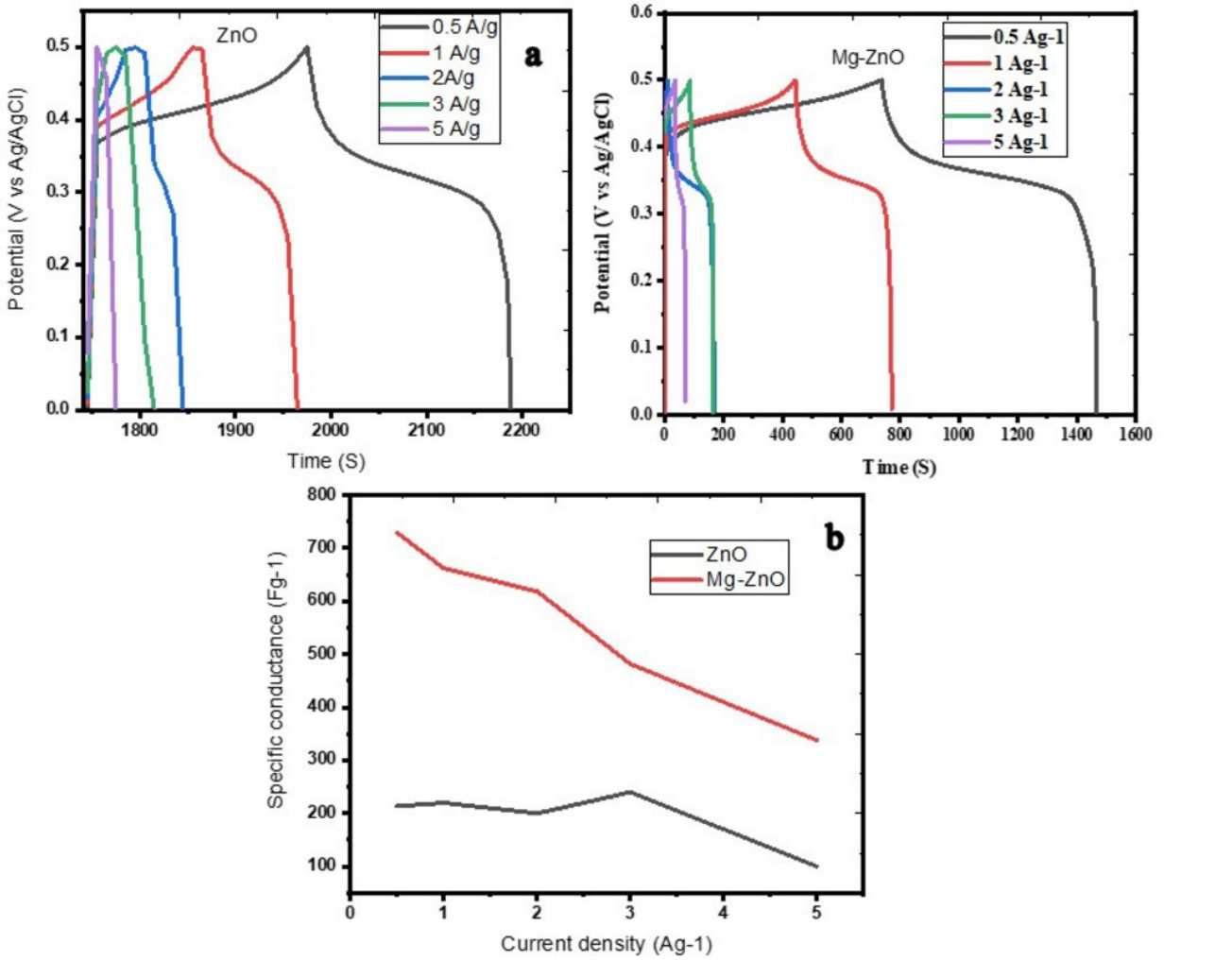

Fig. 7. (a) GCD curves of ZnO and (b) Mg-ZnO calcined at 450°C, (b) Specific conductance vs current density curves of ZnO and Mg-ZnO calcined at 450°C

charge/discharge cyclic stability curves. It is assumed from the GCD curves that the discharge period has increased considerably as the cycles number increases and the trend of the specific capacitance of Mg-doped ZnO with a rise in the cycle number is shown in Fig. 8, reveals the material solidity. Observed steady increase in specific capacitance from 481.8 to 618.4 F g^{-1} and an increase of up to 102 percent of the initial capacitance for 500 cycles at 5 A g^{-1} current density [36].

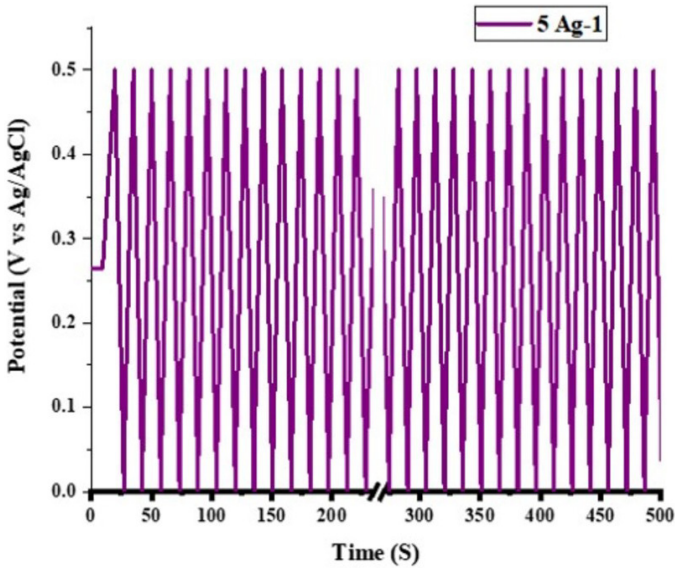

Fig. 8. GCD curves of Mg-ZnO for 500 cycles at current density 5 A g^{-1}

4. Conclusion

Mg-doped zinc oxide has been effectively synthesized using a soft chemical process at room temperature and calcined at 450°C to improve the crystalline nature of the sample. Prepared Mg-doped ZnO was analyzed with XRD, PL, FTIR, and SEM-EDX spectral analysis, which showed spherical morphology with a mean size of particle ~85 nm. In addition, FT-IR shows the potential chemical group present in it, and the elemental composition confirms the purity of the sample. Pseudo-capacitive studies further illustrate the electrochemical properties of Mg-doped ZnO with a higher specific capacitance of 729 F g^{-1} at current density of 0.5 A g^{-1} and maintain a specific capacitance of 100 percent at current density of 2 A g^{-1}. The redox nature of the Mg-doped zinc oxide is one of the pristine candidates for ultra-capacitor applications. In addition, cyclic stability studies showed a steady increase in real capacitance from 481.8 to 618.4 F g^{-1} and an increase of up to 102 percent of the early capacitance for 500 cycles at a current density of 5 A g^{-1}.

Acknowledgement

The authors would like to thank Dr. P. Selvakumar, Vivekanandha College of Arts & Sciences for Women (Autonomous) for his supportive discussions and grateful support.

Funding

The far-red region

This research did not receive any specific grant from funding agencies in the public, commercial, or not-for-profit sectors.

REFERENCES

[1] M. Kim, K.-J. Kim, S.-J. Lee, H.-M. Kim, S.-Y. Cho, M.-S. Kim, S.-H. Kim, K.-B. Kim, ACS Appl. Mater. Interfaces **9** (1), 701-709 (2017). DOI: https://doi.org/10.1021/acsami.6b12622

[2] S. Choi, S. I. Han, D. Kim, T. Hyeon, D.-H. Kim, Chem. Soc. Rev. **48** (6), 1566-1595 (2019). DOI: https://doi.org/10.1039/C8CS00706C

[3] L.H. Madkour, in Nanoelectron. Mater. Springer, 605-699 (2019). DOI: https://doi.org/10.1007/978-3-030-21621-4_16

[4] M. Rafique, M. B. Tahir, I. Sadaf, in Adv. Res. Nanosci. Water Technol. Springer, 95-131 (2019). DOI: https://doi.org/10.1007/978-3-030-02381-2_5

[5] T. Xiao, J. Huang, D. Wang, T. Meng, X. Yang, Talanta **206**, 120210 (2020). DOI: https://doi.org/10.1016/j.talanta.2019.120210

[6] Y. Zhang, X. Xia, B. Liu, S. Deng, D. Xie, Q. Liu, Y. Wang, J. Wu, X. Wang, J. Tu, Adv. Energy Mater. **9** (8), 1803342 (2019). DOI: https://doi.org/10.1002/aenm.201803342

[7] F. Khurshid, M. Jeyavelan, M.S.L. Hudson, S. Nagarajan, R. Soc. Open Sci. **6** (2), 181764 (2019). DOI: https://doi.org/10.1098/rsos.181764

[8] M.M. Sajid, N.A. Shad, Y. Javed, S.B. Khan, N. Amin, Z. Zhang, Z. Imran, M.I. Yousuf, Appl. Nanosci. **10** (2), 421-433 (2020). DOI: https://doi.org/10.1007/s13204-019-01199-8

[9] H. Zeng, X. Zhao, F. Zhao, Y. Park, M. Sillanpää, Chem. Eng. J. **382**, 122972 (2020). DOI: https://doi.org/10.1016/j.cej.2019.122972

[10] L. Zheng, F. Teng, X. Ye, H. Zheng, X. Fang, Adv. Energy Mater. **10** (1), 1902355 (2020). DOI: https://doi.org/10.1002/aenm.201902355

[11] M. Periyasamy, A. Kar, J. Mater. Chem. C **8** (14), 4604-4635 (2020). DOI: https://doi.org/10.1039/C9TC06469A

[12] S.K. Gupta, S. Gupta, A.K. Gupta, Adv. Sci. Eng. Med. **12** (1), 11-26 (2020). DOI: https://doi.org/10.1166/asem.2020.2516

[13] Z. Li, A. Khajepour, J. Song, Energy **182**, 824-839 (2019). DOI: https://doi.org/10.1016/j.energy.2019.06.077

[14] S.A. Hashmi, N. Yadav, M.K. Singh, Polym. Electrolytes Charact. Tech. Energy Appl. 231-297 (2020). DOI: https://doi.org/10.1002/9783527805457.ch9

[15] X. Kong, L. Yang, Z. Cheng, S. Zhang, Materials **13** (1), 180 (2020). DOI: https://doi.org/10.3390/ma13010180

[16] B. Zhao, F. Mattelaer, J. Kint, A. Werbrouck, L. Henderick, M. Minjauw, J. Dendooven, C. Detavernier, Electrochimica Acta **320**, 134604 (2019). DOI: https://doi.org/10.1016/j.electacta.2019.134604

[17] Y. Wang, C. Ma, C. Wang, P. Cheng, L. Xu, L. Lv, H. Zhang, Sol. Energy **189**, 412-420 (2019). DOI: https://doi.org/10.1016/j.solener.2019.07.082

[18] J. Jiang, S. Liu, Y. Wang, Y. Liu, J. Fan, X. Lou, X. Wang, H. Zhang, L. Yang, Chem. Eng. J. **359**, 746-759 (2019). DOI: https://doi.org/10.1016/j.cej.2018.11.190

[19] H.M.A. Javed, W. Que, M.R. Ahmad, K. Ali, M.I. Ahmad, A. ul Haq, S.K. Sharma, in Sol. Cells (Springer, 2020), pp. 25-54. DOI: https://doi.org/10.1007/978-3-030-36354-3

[20] S.E. Arasi, P. Devendran, R. Ranjithkumar, S. Arunpandiyan, A. Arivarasan, Mater. Sci. Semicond. Process. **106**, 104785 (2020). DOI: https://doi.org/10.1016/j.mssp.2019.104785

[21] H.-C. Chen, Y.R. Lyu, A. Fang, G.J. Lee, L. Karuppasamy, J.J. Wu, C.K. Lin, S. Anandan, C.Y. Chen, Nanomaterials **10** (3), 475 (2020). DOI: https://doi.org/10.3390/nano10030475

[22] N. Sivakumar, J. Gajendiran, R. Jayavel, Chem. Phys. Lett. **745**, 137262 (2020). DOI: https://doi.org/10.1016/j.cplett.2020.137262

[23] M.A.F. Mohd Shaifuddin, C.A. Che Abdullah, S.H. Ribut, N.S. Rosli, R. Mohd Zawawi, Malays. J. Sci. Health Technol. (2019). https://oarep.usim.edu.my/jspui/handle/123456789/5353

[24] G. Wu, Y. Song, J. Wan, C. Zhang, F. Yin, J. Alloys Compd. **806**, 464-470 (2019). DOI: https://doi.org/10.1016/j.jallcom.2019.07.175

[25] S. Kasap, I.I. Kaya, S. Repp, E. Erdem, Nanoscale Adv. **1** (7), 2586-2597 (2019). DOI: https://doi.org/10.1039/C9NA00199A

[26] U. Bhat, S. Meti, Graphene-Based ZnO nanocomposites for Supercapacitor Applications in Graphene as Energy Storage Materials for Supercapacitors, Eds. Inamuddin, Rajender Boddula, Mohammad Faraz Ahmer and Abdullah M. Asiri, Materials Research Foundations **64**, 181 (2020). DOI: https://doi.org/10.21741/9781644900550-7

[27] M. Ghosh, S. Mandal, A. Roy, S. Chakrabarty, G. Chakrabarti, S.K. Pradhan, Mater. Sci. Eng. C **106**, 110160 (2020). DOI: https://doi.org/10.1016/j.msec.2019.110160

[28] R. Subbiah, S. Muthukumaran, V. Raja, Optik 164556 (2020). DOI: https://doi.org/10.1016/j.ijleo.2020.164556

[29] R. Sánchez-Tovar, E. Blasco-Tamarit, R.M. Fernández-Domene, M. Villanueva-Pascual, J. García-Antón, Surf. Coat. Technol. 125605 (2020). DOI: https://doi.org/10.1016/j.surfcoat.2020.125605

[30] N. Jayaprakash, R. Suresh, S. Rajalakshmi, S. Raja, E. Sundaravadivel, M. Gayathri, M. Sridharan, Mater. Technol. **35** (2), 112-124 (2020). DOI: https://doi.org/10.1080/10667857.2019.1659533

[31] M. Achehboune, M. Khenfouch, I. Boukhoubza, B.M. Mothudi, I. Zorkani, A. Jorio, J. Mater. Sci. Mater. Electron. **31** (6), 4595-4604 (2020). DOI: https://doi.org/10.1007/s10854-020-03011-8

[32] C.V. Thulasi-Varma, B. Balakrishnan, H.-J. Kim, J. Ind. Eng. Chem. **81**, 294-302 (2020). DOI: https://doi.org/10.1016/j.jiec.2019.09.017

[33] J. Yus, B. Ferrari, A.J. Sanchez-Herencia, Z. Gonzalez, Electrochimica Acta **335**, 135629 (2020). DOI: https://doi.org/10.1016/j.electacta.2020.135629

[34] N. Liu, Z. Pan, X. Ding, J. Yang, G. Xu, L. Li, Q. Wang, M. Liu, Y. Zhang, J. Energy Chem. **41**, 209-215 (2020). DOI: https://doi.org/10.1016/j.jechem.2019.05.008

[35] M. Bolsinger, M. Weller, S. Ruck, P. Kaya, H. Riegel, V. Knoblauch, Electrochimica Acta. **330**, 135163 (2020). DOI: https://doi.org/10.1016/j.electacta.2019.135163

[36] H. Jia, Z. Wang, B. Tawiah, Y. Wang, C.-Y. Chan, B. Fei, F. Pan, Nano Energy **70**, 104523 (2020). DOI: https://doi.org/10.1016/j.nanoen.2020.104523